JOURNAL OF GEOPHYSICAL RESEARCH, VOL. 102, NO. B9, PAGES 20,539-20,550, SEPTEMBER 10, 1997

Three-dimensional dislocation model for great earthquakes of the Cascadia subduction zone

P. Flück,[1,2] R. D. Hyndman,[2] and K. Wang

Geological Survey of Canada, Pacific Geoscience Centre, Sidney, British Columbia, Canada

Abstract. There have been no historical Cascadia great subduction thrust earthquakes, but there is good recent evidence that very large earthquakes have occurred in the past and that strain is building up toward a future great event. Geodetic measurements in the coastal region from northern California to southern British Columbia show vertical and horizontal deformation as expected for the strain accumulation of a locked thrust fault. The segment of the subduction thrust that is locked and may rupture in future great events has previously been estimated through two-dimensional (2-D) elastic dislocation modeling of interseismic deformation geodetic data. In this study, a general 3-D dislocation model for thrust faults has been developed that accommodates curved fault geometry and nonuniform interseismic locking or coseismic rupture. The model is based on the surface deformation due to shear faulting in an elastic half space. The 3-D model of the Cascadia subduction zone calculates the surface deformation for a locked zone or a rupture zone of variable width along the margin. The bend in the margin trend and subducting slab end effects are included. There is a downdip transition zone between interseismic completely locked and free slip portions of the fault or between coseismic full rupture and no displacement. An initial 3-D model based upon 2-D dislocation models and upon thermal constraints was adjusted to optimize the fit of the predicted interseismic surface deformation to current deformation geodetic data. The best fit model has the thrust locked along the whole margin with an average locked zone width of 60 km and a transition zone width of 60 km. The two zones lie mainly offshore beneath the continental shelf and slope. The locked and transition zone widths vary smoothly along the margin, being greater off northern Washington where the thrust dip is shallow and narrower off central Oregon. Assuming that the locked plus transition zones approximate the maximum coseismic rupture area, these widths permit a $M_w = 9$ earthquake.

1. Introduction

The Cascadia continental margin along the southwest coast of Canada and northwest coast of United States (Figure 1) shows most of the features of active subduction zones; a chain of active volcanoes (e.g., Mount St. Helens), Benioff-Wadati seismicity, seismicity in the continental plate, typical gravity and heat flow patterns, a deformed accretionary sedimentary prism, and current vertical deformation and horizontal shortening across the coastal region. A striking difference compared to most subduction zones is the lack of historical great thrust earthquakes. However, clear evidence has been found that great earthquakes have happened in the past, prior to the first written records. The last event was about 300 years ago, and the average time interval is about 500 years. The evidence includes buried coastal marsh deposits indicating abrupt subsidence (summary by *Atwater et al.* [1995]), overlying sand sheets resulting from the associated great tsunami waves, deep-sea turbidite layers resulting from continental slope landslides [*Adams*, 1990], and a tsunami recorded in Japan in the year 1700 with probable Cascadia origin [*Satake et al.*, 1996].

Important supporting evidence for the occurrence of great earthquakes comes from geodetic data indicating ongoing elastic strain buildup of the form expected for a locked subduction thrust fault [e.g., *Hyndman and Wang*, 1995, and references therein]. During the interseismic period the interface between the subducting slab and the overlying continental plate is locked and strain accumulates. There is horizontal shortening across the coastal region. The edge of the continent is dragged down, but an upward flexural bulge forms landward. During a subduction thrust earthquake the horizontal compression across the coastal region relaxes and extends. The continental edge springs back up, and the bulge built up during the interseismic period collapses. The collapse of the bulge causes the abrupt subsidence recorded in the Cascadia coastal marshes. The associated seafloor displacement generates the large tsunami.

The location of the seismogenic source zone on the subduction thrust fault, especially its distance from inland cities, is a critical parameter for seismic risk analysis. The downdip width of the Cascadia thrust locked zone has been estimated from two-dimensional modeling of geodetic data [e.g., *Savage et al.*, 1991; *Dragert et al.*, 1994; *Hyndman and Wang*, 1993, 1995]. A slip deficit is assumed on the locked portion of the thrust plane at a rate equal to the plate convergence rate, which decreases downdip through a transition zone to zero. This slip deficit multiplied by the interseismic period between great events is

[1]Also at Swiss Federal Institute of Technology, Zürich, Switzerland

[2]Also at School of Earth and Ocean Sciences, University of Victoria, Victoria, British Columbia, Canada.

Paper number 97JB01642.
0148-0227/97/97JB-01642$09.00

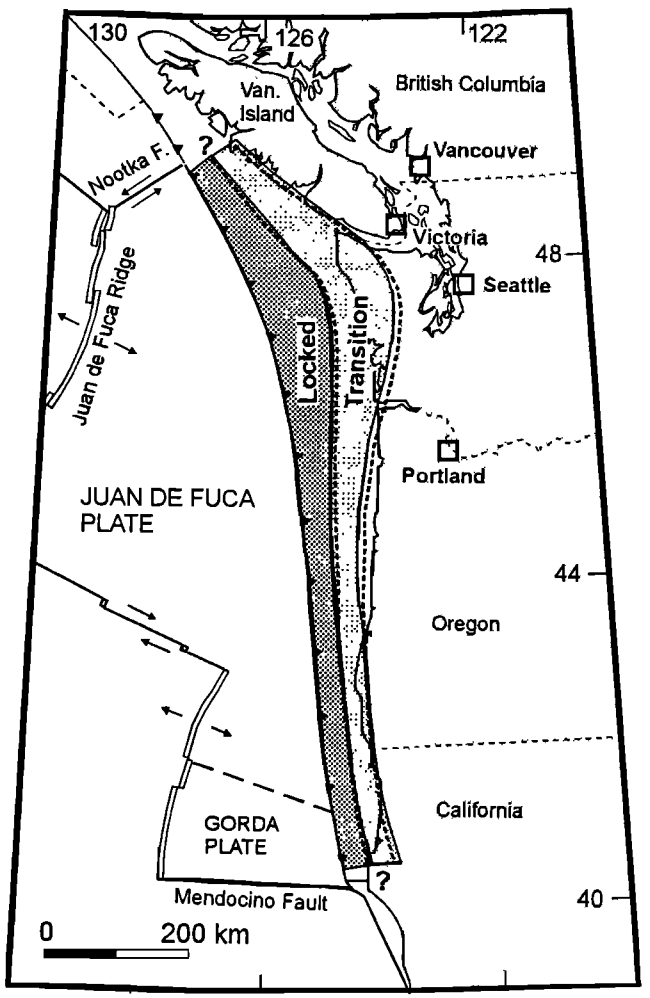

Figure 1. The Cascadia subduction zone. The 3-D model locked and transition zone widths shown shaded provide the best fit to the current deformation data. The dashed lines show the previously estimated widths based on a series of 2-D models.

assumed to equal the coseismic slip. Thus there is no cumulative deformation through several model earthquake cycles, as is approximately observed for the Cascadia margin [e.g., *Kelsey et al.*, 1994]. If a fraction of the fault slip takes place aseismically, then the assumed coseismic fault slip must be reduced by that amount. There are unresolved theoretical questions regarding using an elastic dislocation model for interseismic deformation [e.g., *Wang*, 1995; *Douglass and Buffett*, 1995, 1996; *Savage*, 1996]. Given the distribution of slip rates on the fault, this kinematic model predicts surface deformation rates but does not predict how the fault slip occurs. Models for the complete earthquake cycle with a more realistic nonelastic rheology and with time dependent deformation through the interseismic period are needed [e.g., *Savage and Thatcher*, 1992; *Wang et al.*, 1994], but considerable work is still necessary for such models to be realistic. However, for several regions the estimated width of coseismic rupture corresponds well to the downdip width of the locked zone from elastic dislocation modeling of interseismic strain data. Comparisons are available for the Nankai margin of southwest Japan [*Hyndman et al.*, 1995] and several other subduction zone margins that have experienced recorded great earthquakes [e.g., *Savage and Plafker*, 1991; *Oleskevich*, 1996]. Thus we take the downdip width of the locked zone (and the transition zone if one is included), determined from dislocation models of interseismic deformation data, to approximate the maximum downdip rupture width in great earthquakes.

The downdip width of the locked seismogenic zones may be controlled by several physical limits. For subduction of young hot oceanic crust beneath continental crust the downdip limit appears to be thermally controlled [e.g., *Hyndman and Wang*, 1993; *Tichelaar and Ruff*, 1993]. The temperature limit of seismic slip for most crustal rocks is about 350°C from laboratory data and from the maximum depth of continental crustal earthquakes. Great earthquakes initiated at temperature less than this limit may extend with decreasing offset through a transition zone to a second downdip limit of about 450°C. At still greater temperatures there is a rapid increase in instantaneous shear stress in laboratory data, and the fault zone material is inferred to behave plastically. For Cascadia [e.g., *Hyndman and Wang*, 1995] and SW Japan [*Hyndman et al.*, 1995; *Wang et al.*, 1995] the downdip limits at these temperatures from thermal modeling are in good agreement with the results of elastic dislocation models constrained by geodetic data. For subduction beneath oceanic crust the downdip limit may be the forearc Moho which is aseismic because of the presence of mantle serpentinite [*Hyndman et al.*, 1997].

There also may be an updip limit to the seismogenic zone commonly associated with the unconsolidated accretionary prism sediments [e.g., *Byrne et al.*, 1988]. This limit has been associated with the presence of stable sliding clays in the fault zone by *Vrolijk* [1990] and *Hyndman et al.* [1997]; such clays dehydrate at 100-150°C . The initial thrust temperatures on the Cascadia margin are unusually high, over 200°C, because of the young oceanic plate age and thick insulating sediment cover on the incoming oceanic crust. Thus, if the 100-150°C temperature limit applies, the seaward boundary of the Cascadia seismogenic zone is at the axis of subduction located at the base of the continental slope, and there is no significant updip aseismic zone. If there are only low concentrations of clay, as is the case for much of the Cascadia accretionary prism [e.g., *Westbrook et al.*, 1994], then there may be no updip aseismic slip zone regardless of the temperature. However, the situation is complicated by the presence of very high pore fluid pressures on the fault [e.g., *Hyndman et al.*, 1994], by the low strength of the unconsolidated seaward prism sediments, and by convergence being accommodated through the bulk deformation shortening of the seaward portion of the prism.

2. Three-Dimensional Dislocation Model

Two-dimensional (2-D) dislocation models [e.g., *Savage, 1983*] have previously been used to model the surface deformation associated with the locked Cascadia subduction thrust [*Savage et al.*, 1991; *Hyndman and Wang*, 1993, 1995; *Dragert et al.*, 1994; *Dragert and Hyndman*, 1995]. The data for model constraint come from long-term tide gauges, repeated precision leveling surveys, laser trilateration surveys, repeated precision gravity measurements, and continuous and repeated Global Positioning System (GPS) surveys. Although of variable type and quality, the Cascadia subduction zone has one of the best defined patterns of interseismic deformation. Deformation data are distributed along the whole margin from Vancouver Island to northern California. A single model, with smooth variation of the locked and transition zone widths along the margin, has predicted surface deformations that fit all of the

available geodetic data within the data uncertainties [*Hyndman and Wang*, 1995].

Verdonck [1995] developed a simple planar rectangular 3-D model with a downdip transition zone for the southern part of the Cascadia subduction zone. Away from the northern and southern ends, the model deformation is similar to that for the 2-D models, and the predicted deformation is in good agreement with data from northern California and southern Oregon. However, this model cannot be applied to a curved subduction zone such as at northern Cascadia or to locked and transition zones that vary in width along the margin. To allow for more complex three-dimensional fault planes, we have developed a general 3-D model. For Cascadia we require the effects on the earthquake cycle deformation of (1) the corner or bend in the subduction zone, (2) locked and transition zone downdip widths that vary along the margin, and (3) the north and south subducting plate edges.

Our three-dimensional dislocation model is based on the point source solution by *Okada* [1985]. Only an outline is given here. More details are given by *Flück* [1996], and the computer routine is available from the authors. To obtain the deformation at each location on the surface, point source dislocations are numerically integrated over the fault plane. For numerical integration the fault plane is divided into a number of planar triangular elements each having an area sufficiently small to approximate a point source located at its center of mass. The solution for deformation at a surface observation point is obtained by summation of the point source solutions over all triangular elements. Any fault geometry and nonuniform slip distributions on the fault can be approximated. For example, the transition zone was modeled by a linear downdip change in dislocation magnitude on the triangle elements.

The computation procedure was first tested by comparison with the analytical solution for a rectangular fault by *Okada* [1985]. This comparison also provided an indication of the maximum size of triangle that gives adequate numerical accuracy while minimizing computing time. The 3-D model deformation was obtained for a test rectangular dislocation 200 km along strike by 50 km downdip and with a 12° dip starting from a depth of 2 km. For 20,000 triangles of size 0.5 km^2 the results are indistinguishable from the analytical solution. The triangle size is particularly important if the fault plane reaches near to the surface. The 3-D solution for a rectangular fault that is very long along strike also reproduces 2-D model results. A detailed analysis examining the effects of varying the main computational parameters is given by *Flück* [1996].

3. Model of Cascadia Subduction Thrust Fault

3.1 Geometry of Subduction Thrust Fault

The 3-D model for the Cascadia subduction zone requires well-defined spatial geometry for the subduction thrust fault. We have assumed that the fault is at the top of the underthrusting Juan de Fuca plate. Near the trench the thrust detachment may be within the accretionary sedimentary prism several hundred meters above the top of the oceanic crust. However, this has little effect on the model surface deformation except seaward near the base of the continental slope, where the exact fault position is important for tsunami generation. In this study we have used the thrust plane constraints compiled by *Hyndman and Wang* [1995] updated with a few additional data. The depth contour lines have been defined by Benioff-Wadati seismicity, seismic reflection, seismic refraction, teleseismic waveform analysis and seismic tomography. Extensive seismicity data are available for British Columbia, Washington, and northernmost California, but there are very few data for Oregon. Benioff-Wadati earthquake hypocenters are restricted to a thin core within the young and thin downgoing plate, and we have assumed that the center of the seismicity is 10 km deeper than the top of the plate. For this work the thrust geometry to about 30 km depth is important, where the thrust fault is locked and will rupture in future great earthquakes. The model fault extends to 50 km depth. The updip end of the subduction thrust is taken to be at the base of the continental slope where the first sediment deformation occurs, as estimated from bathymetry and seismic reflection data. Models for the seaward most part of the thrust that affects tsunami generation are discussed in Section 5. Figure 2 shows the contour lines of the subducting slab; the lines are solid are where the depths are well constrained and dashed where the depths are poorly constrained.

For the Vancouver Island margin the top of the downgoing plate is well defined from the multichannel seismic reflection and refraction data to a depth of about 30 km [*Green et al.*, 1990; *Hyndman et al.*, 1990; *Spence et al.*, 1991; *Hyndman et al.*, 1994; *Hyndman*, 1995]. The reflection thrust profile is in good agreement with the depths of Benioff-Wadati earthquakes [*Rogers*, 1994] and with the position of the downgoing plate from receiver function analyses of teleseismic broadband data [*Cassidy and Ellis*, 1993; *Cassidy*, 1995; *Bostock and Van Decar*, 1995]. For the Washington margin the depth of the seaward part of the slab is constrained by seismic reflection data [e.g., *Snavely*, 1987], but the depth farther landward is mainly from the strong Benioff-Wadati seismicity. The earthquake hypocenters and receiver function studies of teleseismic converted *P-S* waves

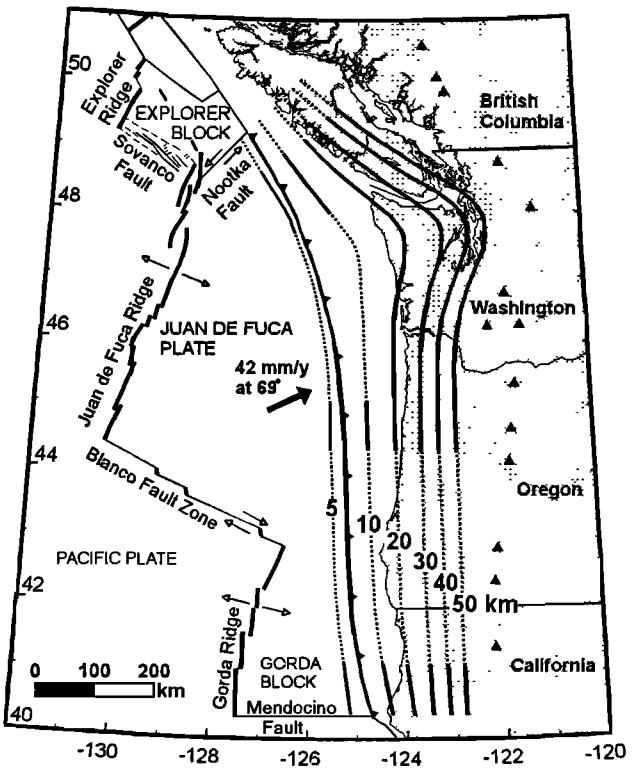

Figure 2. Contours of Cascadia subduction thrust fault depth from seismic reflection and refraction, Benioff-Wadai seismicity, teleseismic waveform analysis, and seismic tomography. Triangles, arc volcano centers; solid lines, depths well constrained; dashed lines, depths poorly constrained.

define the subducting plate depths well between 20 and 60 km [*Crosson and Owens*, 1987]. Other interpretations of the seismicity give similar results [*Taber and Lewis*, 1986; *Weaver and Baker*, 1988, *Rieken and Thiessen*, 1992], as do other teleseismic waveform analyses [*Owens et al.*, 1988; *Rasmussen and Humphreys*, 1988; *Lapp et al.*, 1990]. For the mid-Oregon margin there is almost no Benioff-Wadati seismicity, but seismic reflection and refraction data provide constraints to 50 km [*MacKay et al.*, 1992; *Trehu et al.*, 1994]. *Nabelek et al.* [1996] also provided receiver function analyses of teleseismic data that define a nearly identical position for the top of the subducting plate. The geometry of the thrust at the southern end of the Cascadia subduction zone is defined from the Benioff-Wadati seismicity [*Jachens and Griscom*, 1983; *Smith et al.*, 1993; *Wang and Rogers*, 1994] and seismic reflection and refraction data [*Trehu et al.*, 1995], although there is some uncertainty in the relation of seismicity to the thrust plane near the southern end of the subduction zone.

We estimate that the contour map of the subduction thrust has an uncertainty of ±0.5 km at the seaward end, increasing to about ±5 km for depths of 50 km. Where the geometry is complex, at the north and south ends and at the margin corner, quite good data are available. There are no breaks or abrupt bends in the plate parallel to the margin evident in the data. The expected plate flattening at the margin corner of the Olympic Peninsula is well defined, but the plate appears to steepen at greater depths.

3.2 Plate Convergence Rate and Direction

Additional important factors in the dislocation model are the direction and magnitude of plate convergence. In the interseismic period between great events the plate convergence defines the dislocation rate at each model point (triangle element). In the model the amount and direction of coseismic slip in a great earthquake are the plate convergence multiplied by the average time between successive events. The current Juan de Fuca plate convergence rate and direction vary by relatively small amounts along the margin. *Riddihough* [1984] estimated a decrease from southern Vancouver Island to Cape Blanco off southern Oregon from 47 to 37 mm yr^{-1}. *DeMets et al.* [1990, 1994] estimated a slightly slower present convergence rate of 42 mm yr^{-1} and a more clockwise (N69°E) convergence direction for the Washington margin. In the model the slip is taken to be 42 mm yr^{-1} at an azimuth of 69°. Subduction is slightly more oblique in the southernmost portion of the region because of the rotation of the Juan de Fuca plate [*Wilson*, 1993]. In the transition zone the model rate decreases downdip linearly to zero. A series of test models has shown that small changes in slip rate of a few millimeters per year and in slip direction of a few degrees have an insignificant effect on the predicted surface deformations, so variations along the margin have been ignored.

The convergence rate and direction off northern California (Gorda Plate) and off northern Vancouver Island north of the Nootka transform fault (Explorer Plate) are not well known. In both areas the oceanic plate appears to be breaking up and the tectonic regime is complex [e.g., *Riddihough*, 1980; *Wilson*, 1989, 1993; *Rohr and Furlong*, 1995; R. Govers et al., The Explorer region: A case study of the dynamics of subduction-spreading-transform triple junction, submitted to *Journal of Geophysical Research*, 1996]. We have included northern California (Gorda Plate) in the model because there are geodetic data indicating convergence. We have excluded northern Vancouver Island (Explorer Plate). *Riddihough* [1984] estimated convergence in a northeasterly direction for the Explorer Plate at a rate about half that of the Juan de Fuca Plate. However, *Rohr and Furlong* [1995] presented evidence that a broad fault zone has broken through the Explorer Plate very recently so that there is little or no present convergence. As yet there are no adequate geodetic data to test this latter hypothesis.

4. Three-Dimensional Dislocation Model of the Cascadia Seismogenic Zone

The downdip extent of the Cascadia locked seismogenic zone has been estimated using the 3-D model. The thrust fault area, fault dislocation direction, and dislocation magnitude were assigned as described above. The updip limit of the locked zone is taken to be at the base of the continental slope (trench); thus the main remaining model variables are the downdip limits of the locked and transition zones. The best constraint on the width of the transition versus the width of the locked zone is the amplitude of the peak vertical deformation; the wider the transition zone, the lower and broader the peak uplift. However, the relative widths of the locked and transition zones are not well constrained separately with the available geodetic data. For most of the region where data are available there is very little difference in the vertical deformation predicted by models with a transition zone and those with no transition zone but with the fully locked zone extended downdip by half the width of the transition zone (e.g., discussion by *Dragert et al.* [1994]). The leveling profiles that do extend seaward of the uplift peak are linked short lines and thus of low quality (located in Washington, to the north and south of the Olympic Peninsula), but they show the peak amplitude expected for a transition zone width comparable to that of the locked zone (see below). We have followed *Hyndman and Wang* [1995], who took the locked and transition zones to be of equal width based primarily on thermal constraints.

The starting 3-D model is a smooth interpolation of the 2-D model locked and transition zones of *Hyndman and Wang* [1995] (Figure 1). Based on the conclusion that the seismogenic zone is thermally limited and that the thermal regime is unlikely to change over short distances, we have taken the smoothest locked and transition zones along the margin that fit the deformation data. More complex models that have rapid variations in widths along the margin are allowed but are not required by the data. More complex models can be easily handled by our 3-D dislocation computation procedure as more data become available. Since we conclude that the downdip limits of the seismogenic zone are thermally controlled, the limits depend mainly on the fault depth. Where the dip is shallower, the critical temperatures are reached farther landward, and the locked and transition zones are wider. Consequently, the zones are wider in the corner of the Olympic Peninsula where the dip is shallower compared to the north and south.

4.1. Thrust Plane Approximation

In the model the medium is a uniform elastic half-space with a flat upper surface. Although the real structure (Figure 3a) cannot be represented accurately by an elastic half-space, Figure 3b shows a better approximation than taking sea level as the half-space surface. First, we have approximated the subduction thrust plane section by smooth downdip profiles for the depth range of the locked and transition zones. Second, the model fault is raised to approximate the depth below a smoothed representation of the seafloor and land surface. The depth below the free surface and the dip angle relative to the free surface, which is ground surface on land and the seafloor offshore, are

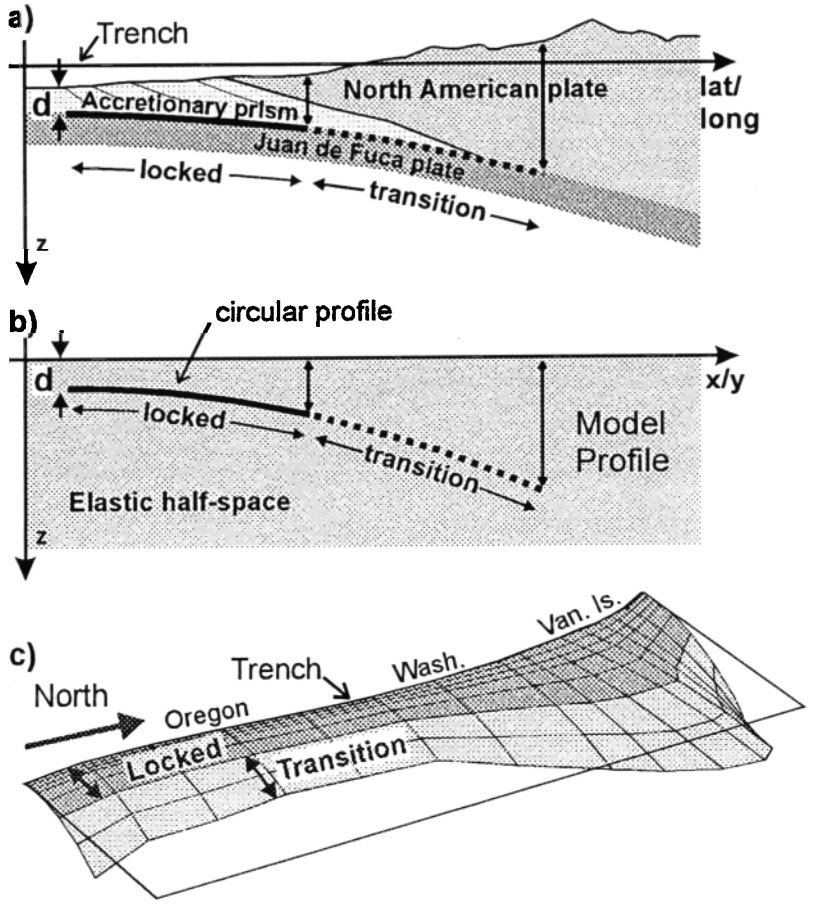

Figure 3. The Cascadia subduction thrust locked and transition zones. (a) Example cross section with actual geometry, (b) geometry approximation used in 3-D dislocation model that corrects for surface topography, and (c) three-dimensional view of the locked and transition zones (view from southeast; 2.5:1 vertical exaggeration).

then correct. We modify the fault dip angle to satisfy the fault depth below the seafloor because what is important is the dip angle relative to the free surface, not the angle relative to sea level. Given the half-space model constraint that the upper surface must be flat, this provides the best approximation.

The initial fault grid has 128 points and 105 quadrilateral elements (Figure 3c), defined by the trench, the downdip edge of the locked zone, and the downdip edge of the transition zone. A denser grid was created by dividing each quadrilateral element into 1000 approximately equally sized triangular elements. There are then 53,321 nodal points and 105,000 triangles approximating the fault plane. The triangle sizes increase downdip from less than 0.5 km^2 at the trench updip edge.

4.2. Three-Dimensional Model Results

The 3-D model vertical and horizontal interseismic deformation patterns for the whole Cascadia subduction zone are shown as contours in Figure 4. The maximum coseismic deformations are given by these rates times the interseismic strain accumulation period, i.e., approximately times 500 years. The interseismic uplift pattern of Figure 4 reaches slightly higher values at the north and south ends where the locked and transition zones are narrower. The uplift is broader and slightly lower in the middle at the corner of the subduction zone where the zones are wider. The updip region near the trench, which is important for tsunami generation, is discussed in Section 5.

Figure 4 shows vectors and contours representing interseismic horizontal velocity and direction. Again, the maximum coseismic displacements are given by these contours times the interseismic period. The magnitude of horizontal motion decreases landward from the trench. At the margin corner the vectors deviate slightly away from the corner, especially inland of the coast. Figure 5a shows the 3-D model interseismic uplift for three profiles perpendicular to the margin (locations in Figure 4). The model widths range from about 35 + 35 km for the Oregon profile, 50 + 50 km for the Vancouver Island profile, and 100 + 100 km for the northern Washington (Olympic Peninsula) profile.

4.3. Comparison of Interseismic Model Results With Current Deformation Data

As discussed above, the deformation between great earthquakes involves complex processes including viscoelastic components. However, with the following assumptions, elastic dislocation models are a useful approximation for comparison with observed deformation during the interseismic period (see discussion above):

1. Earthquake cycles can be approximated by elastic behavior.
2. There is no net permanent deformation through a complete cycle of strain buildup and earthquake release.
3. Surface deformation depends directly upon convergence velocity and thus slip rate on the deeper aseismic part of the subduction thrust fault.

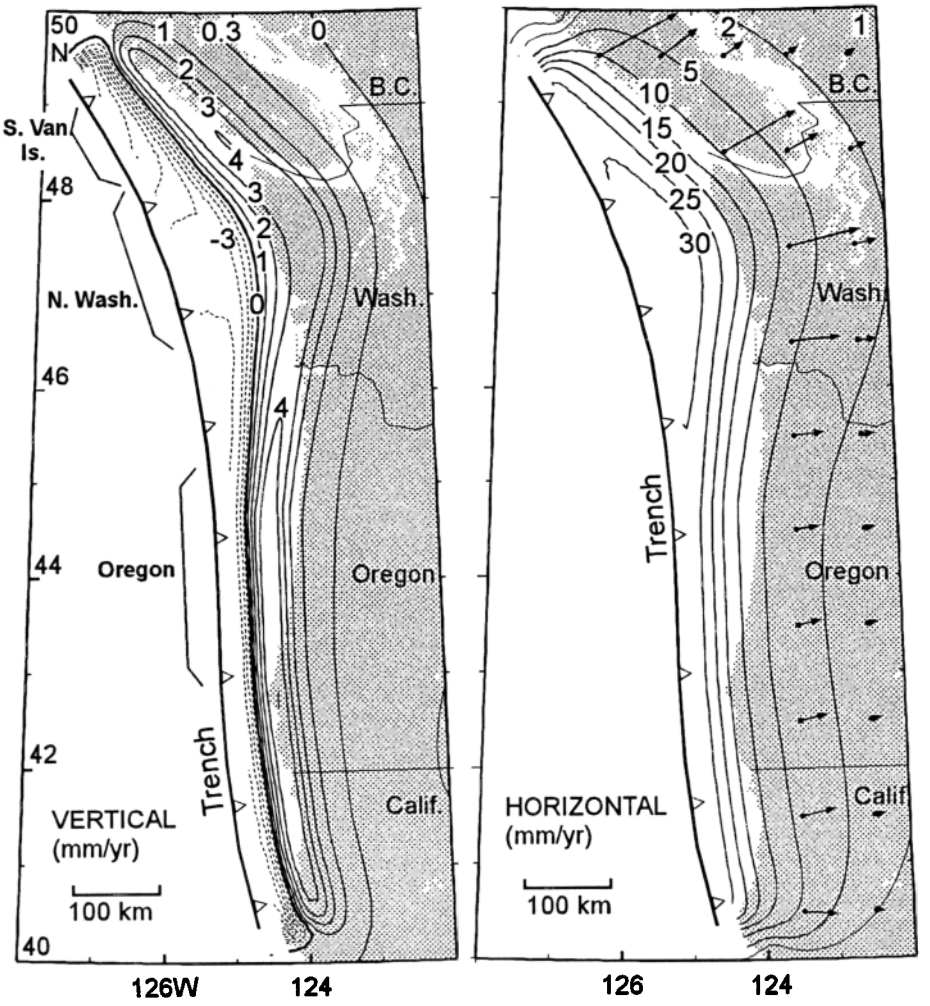

Figure 4. (left) Contours of interseismic uplift rates (mm/yr) predicted by the 3-D dislocation model. (right) Vector directions and contours of magnitude of horizontal velocity (mm/yr). The arrow lengths are proportional to the rate at their origin points. The locations of the groups of leveling lines and tide gauges of Figure 5 are shown as S. Van. Is., N. Wash., and Oregon.

4. The interseismic slip velocity in the locked zone is zero, increasing landward in the transition zone to the full plate convergence rate.

5. The surface deformation rate is constant at the present rate through the interseismic period (except for a transient lasting a few years after great earthquakes).

6. Locked and transition zone areas do not change through the interseismic period.

The vertical and horizontal current deformation data available for comparison with the Cascadia dislocation model have been described by *Hyndman and Wang* [1995] and others, and only a brief summary is given here. An important advantage of the 3-D model is that the deformation is predicted for all points. It is not necessary to project the data onto model profiles across the margin. For vertical deformation, the data include repeated leveling [*Ando and Balazs*, 1979; *Reilinger and Adams*, 1982; *Dragert and Lisowski*, 1990; *Holdahl et al.*, 1989; *Dragert et al.*, 1994; *Mitchell et al.*, 1994], repeated gravity [*Dragert et al.*, 1994], long-term trends in tide gauge data [*Savage et al.*, 1991; *Riddihough*, 1982; *Clague et al.*, 1982; *Holdahl et al.*, 1989; *Dragert et al.*, 1994; *Mitchell et al.*, 1994], and vertical Global Positioning System (GPS) [*Dragert and Hyndman*, 1995]. For horizontal deformation, the data include triangulation-trilateration laser ranging [*Lisowski et al.*, 1989; *Dragert and Lisowski*, 1990; *Savage et al.*, 1981, 1991; *Snay and Matsikari*, 1991; *Dragert et al.*, 1994] and continuous GPS recording stations [*Dragert and Hyndman*, 1995; *Henton et al.*, 1997]. All data have been used to estimate the best locked and transition zone widths along the margin. However, for presentation, we give a selection of the better data from the compilation by *Hyndman and Wang* [1995]. The vertical data on profiles roughly perpendicular to the margin have been combined into three groups representing southern Vancouver Island, northern Washington, and central Oregon (Figure 5a) (see *Mitchell et al.* [1994] and *Hyndman and Wang* [1995] for line locations and data details). Some of the three-dimensional character of the data is thus lost in this presentation, but the three-dimensional variations have been used in the model constraint.

The linked leveling lines lying approximately along the coast are also presented [*Mitchell et al.*, 1994] (Figure 5b). These data provide an important constraint to the 3-D model, but unfortunately, these leveling data have a large uncertainty. Error propagation along the lines is such that they must be tied to tide gauge data to constrain the long spatial wavelength trends. The revision to the tide gauge interpretation on the coast of central Washington by *Hyndman and Wang* [1995] is assumed; there is

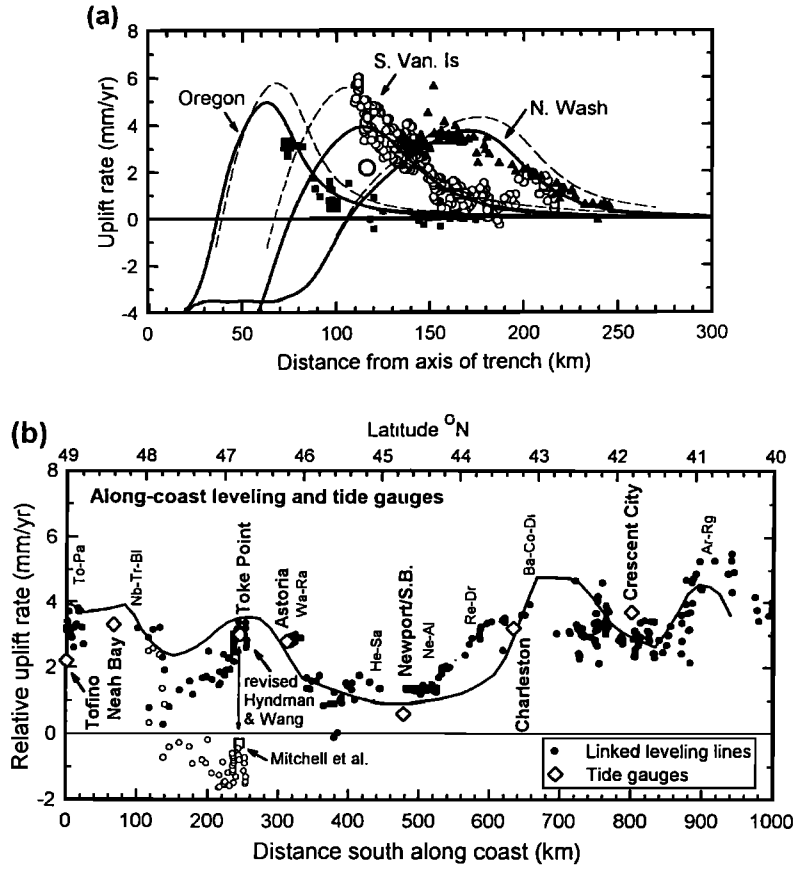

Figure 5. Uplift data compared to predictions from 3-D model. (a) Leveling and tide gauge data in the region of three profiles across the margin. The dashed lines are the 2-D results of *Hyndman and Wang* [1995]. The data locations are shown in Figure 4. (b) Linked leveling lines that run approximately along the coast and associated tide gauge sites (data modified from *Mitchell et al.* [1994]).

an especially large uncertainty on this portion of the profile. Continuous recording GPS horizontal data for stations across the Vancouver Island margin are also presented, updated and extended from *Dragert and Hyndman* [1995] (H. Dragert and J. Henton, personal communication, 1996] (Figure 6).

The locked and transition zones based on previous 2-D model results [after *Hyndman and Wang*, 1995] and the refined 3-D model results that best fit the current deformation data are shown in Figure 1. The changes are small; the new best fitting model has slightly narrower zones off central Oregon and slightly wider off southern Vancouver Island compared to the previous model.

5. Three-Dimensional Dislocation Model of Coseismic Deformation and Tsunami Generation

5.1 Coseismic Deformation

There are no historical records of great earthquakes on the Cascadia subduction zone. Thus coseismic deformation and the tsunami generation must be estimated from (1) paleoseismicity data of coastal downdrop, (2) paleotsunami data of wave runup effects, and (3) models of coseismic seafloor deformation. Historical records in Japan of the waves generated by the last great Cascadia earthquake [*Satake et al.*, 1996] also provide a constraint. In this study we estimate the seafloor coseismic displacement from the 3-D elastic dislocation models, assuming that the thrust fault rupture area is the same as the interseismic locked (and transition) zone, i.e., all of the locked and transition zone rupture in a single event. The estimated coseismic rupture also provides information on the abrupt coastal subsidence which is an important hazard, and for models of the ground motion generated by the earthquake.

We have estimated the coseismic deformation (Figure 4) from the interseismic locked zone models with the following assumptions: (1) There is no net deformation over a great earthquake cycle, (2) the interseismic plate convergence and strain accumulation are constant over time, (3) the last great earthquake released all the elastic strain accumulated in the preceding interseismic period, (4) the coseismic slip is the negative product of plate convergence rate and the interval between two great earthquakes, and (5) there is total rupture of the locked zone (and transition zone with displacement decreasing downdip) along the whole Cascadia margin.

5.2. Comparison With Paleoseismicity Subsidence Data

The coseismic subsidence from the 3-D model may be compared to that estimated from buried coastal marsh data and other indicators of coseismic coastal subsidence. Assuming that the most recent great earthquake released all of the elastic strain accumulated as a result of plate convergence in the preceding interseismic period, the expected coseismic subsidence equals the mean model uplift rate times the interseismic period. Table 1 gives the inferred subsidence for an average interseismic period

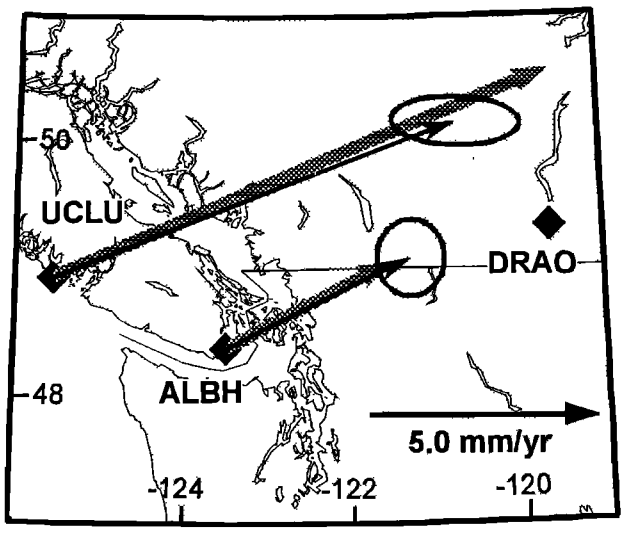

Figure 6. Horizontal velocities from 3-D model compared with the measured values from continuous GPS data at two sites ALBH and UCLU, relative to inland site DRAO (data from *Henton et al.* [1997]). The model values are thick shaded arrows; the measured values are thin arrows with 95% uncertainties.

of 500 years. The most recent event was about 300 years ago, and the previous clear event was over 900 years ago according to coastal data [e.g., *Atwater et al.*, 1995] for an interval of 600-700 years. There is evidence for an intermediate event about 690 years ago (390 year interval) in the deep sea turbidite data [*Adams*, 1990] and there is some limited evidence in the coastal marsh data [*Clague and Bobrowsky*, 1994]. For much of the coast the present uplift rate is 3-4 mm yr^{-1} so the longer interval gives a subsidence of about 1.8-2.8 m. If an intermediate event occurred, the predicted coseismic subsidence will be 1.2-1.6 m. For the coast of central Oregon where the present model uplift rate is about 1 mm yr^{-1} the predicted coseismic subsidence is 0.6-0.7 m for the longer interseismic interval and 0.4 m for the shorter interval. These subsidence values are slightly larger but similar to those inferred from coastal data, with the smallest subsidence on the central Oregon coast and larger values to the north and south.

The coseismic coastal subsidence may be estimated from the depth interval between the present coastal marsh surface (present sea level) and the previous marsh top (sea level prior to the event), allowing for three factors: (1) The earthquake cycle interseismic uplift since the last event, (2) the global eustatic sea level rise since the last event, and (3) the postglacial rebound since the last event. An initial estimate by *Hyndman and Wang* [1995] of these corrections gives general agreement with the vertical interval between the present and next previous marsh. An improved estimate is available from analysis of paleoenvironment indicators of water depth above and below coastal marsh sequences buried by the last great event [e.g., *Atwater et al.*, 1995; *Guibault et al.*, 1996]. The water depth contrasts are mostly somewhat smaller but are in approximate agreement with the dislocation model predictions for the most recent event. For example, *Guibault et al.* [1996] found the difference to lie between 0.2 and 1.0 m for the west coast of Vancouver Island where the dislocation model predicts 1.2-1.6 m. This comparison is an important direction for further study.

5.3. Updip Fault Geometry and Tsunami Generation

The tsunami generated by a great earthquake is strongly dependent upon the updip geometry of the subduction thrust fault near the toe of the accretionary prism. In tsunami modeling, the coseismic displacement of the water surface is the important source function. This sea surface displacement is approximately the same as the coseismic deformation of the seafloor [e.g., *Priest*, 1995; *Geist and Yoshioka*, 1996]. The effect of horizontal displacement can usually be neglected, except for a tsunami source on a steep slope and for a horizontal deformation component that is large relative to the vertical component [*Tanioka and Satake*, 1996]. Tsunami generation from Cascadia great earthquakes is limited mainly to the region over the continental slope where the seafloor gradient is quite low, and thus the vertical deformation probably dominates. For the simplest geometry in the 3-D model, full rupture extends updip to the seafloor. The coseismic seafloor displacements were determined for five alternative fault geometries and slip distributions that might better approximate shallow coseismic rupture (Figure 7). In each case the downdip limits of the locked and transition zones vary along the margin as in the simple model.

The fault slip distribution in Figure 7a is the same as the model used for estimating the interseismic deformation on land; the full coseismic slip is 21 m, and the downdip transition zone has slip that decreases downdip from 21 m to 0 m. The fault slip in Figure 7b has an updip transition zone with a width that is 20% of the full rupture downdip width. This approximation recognizes that near the trench much of the convergence is accommodated by shortening of the accretionary prism sediments rather than slip on the subduction thrust. The relatively unconsolidated sediments at the seaward portion of the accretionary prism also may not allow slip on the fault at seismic rupture speeds. The fault slip distributions in Figures 7c, 7d, and 7e allow for the listric geometry of the frontal thrusts that rise to the seafloor at the base of the continental slope in many multichannel seismic reflection lines [e.g., *Davis and Hyndman*, 1989; *MacKay et al.*, 1992]. The updip region of the deformation front is actually complex and highly variable along the margin. In different areas, shortening is accommodated by landward dipping listric faults, seaward dipping thrusts, folds, and pervasive bulk shortening. For the fault geometry in Figure 7c, rupture propagates with full slip along the listric fault to the surface at the trench. The fault geometry in Figure 7d has a transition in slip in the listric portion from 21 m to 0 m. For the fault geometry in Figure 7e the transition in slip is over the updip 20% of the area of full rupture

Table 1. Coseismic Deformation From 3-D Model for Major Cities and Coastal Sites Along the Cascadia Margin

Location	Horizontal Displacement, m	Azimuth, deg	Subsidence, m
Vancouver	1.0	236	0.01
Victoria	2.2	240	0.21
Seattle	1.4	255	0.05
Portland	1.2	264	0.05
Tofino (TO)	5.4	242	1.9
Neah Bay (NB)	6.1	244	2.0
Astoria (AS)	4.3	259	1.2
Charleston (CH)	5.8	252	2.3
Crescent City	5.3	252	2.2

Complete release of the strain built up during an interseismic period of 500 years is assumed.

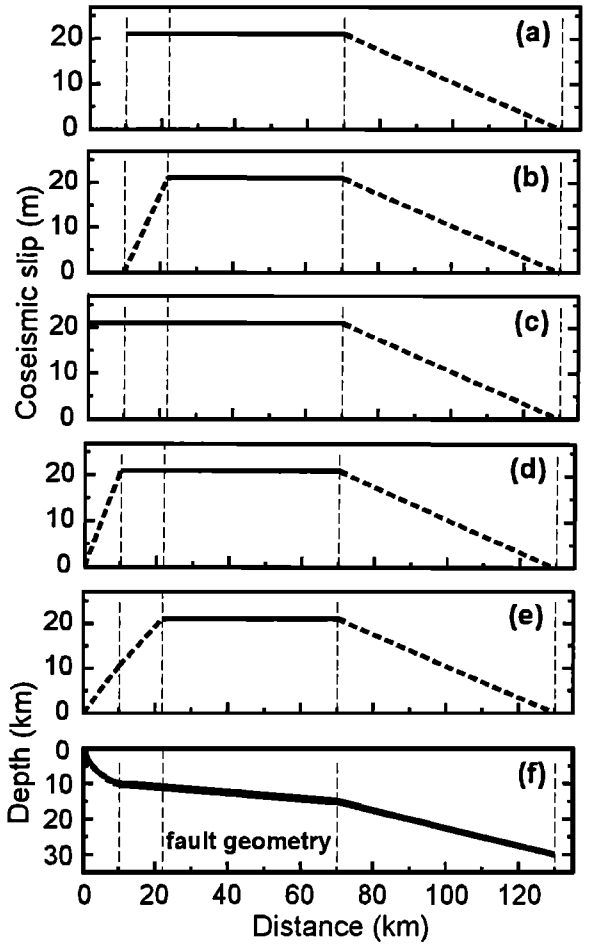

Figure 7. (a)-(e) Updip slip distributions for different models to examine the effect on seafloor deformation and thus coseismic tsunami generation. The solid lines represent areas of full slip, and the dashed lines are zones of transition from full to zero slip. (f) The fault geometry.

in the fault of Figure 7a. The geometry of the listric fault is taken from one portion of the margin where it is approximated by a circle with a radius of 16 km tangent to the deeper fault plane [e.g., *Davis and Hyndman*, 1989].

Because these fault models reach the surface, the triangle element size must be smaller than for the deeper part of the fault to allow accurate numerical integration. A triangle size of 0.03 km^2 was used, requiring 340,800 triangles in the listric portion. The vertical uplift with distance over the first 50 km landward from the trench is given for Vancouver Island (where widths are 60 + 60 km), Washington (100 + 100) and Oregon (40 + 40) in Figure 8. In all cases the uplift landward of about 30 km from the trench is unaffected by variations in seaward geometry. Farther landward the uplift is as previously given in Figure 4 for the Figure 7a geometry. The model in Figure 7c has a singularity in uplift and has the narrowest uplift because full rupture comes to the surface. For the models in Figures 7d, 7a, and 7b the peak uplift moves progressively landward with transition zones that are successively wider. The double peak for the fault slip in Figure 7e applied to the Washington profile is caused by the change in slip gradient for the two parts of the updip transition zone. The scenarios given show a range of possible vertical deformation of the seafloor and thus of displacement of the water surface that may be used for tsunami modeling.

6. Discussion

The differences between the predicted pattern of surface deformation for the three dimensional slip in the Cascadia subduction zone, compared to those from a series of 2-D models spaced along the margin, are relatively small. In detail, the 3-D model provides more accurate deformation estimates in the margin corner and gives predicted patterns of deformation at the north and south ends of the subduction zone. The influence of the locked thrust fault extends only about 20 km from the north and south ends of the subducting plate. An important value of the three dimensional model is that it allows comparison of geodetic data with model predictions at any point along the margin, without projection onto two-dimensional profiles.

A single 3-D model with a smooth variation along the margin in locked and transition zone widths fits most of the available current deformation data, both vertical and horizontal, within the

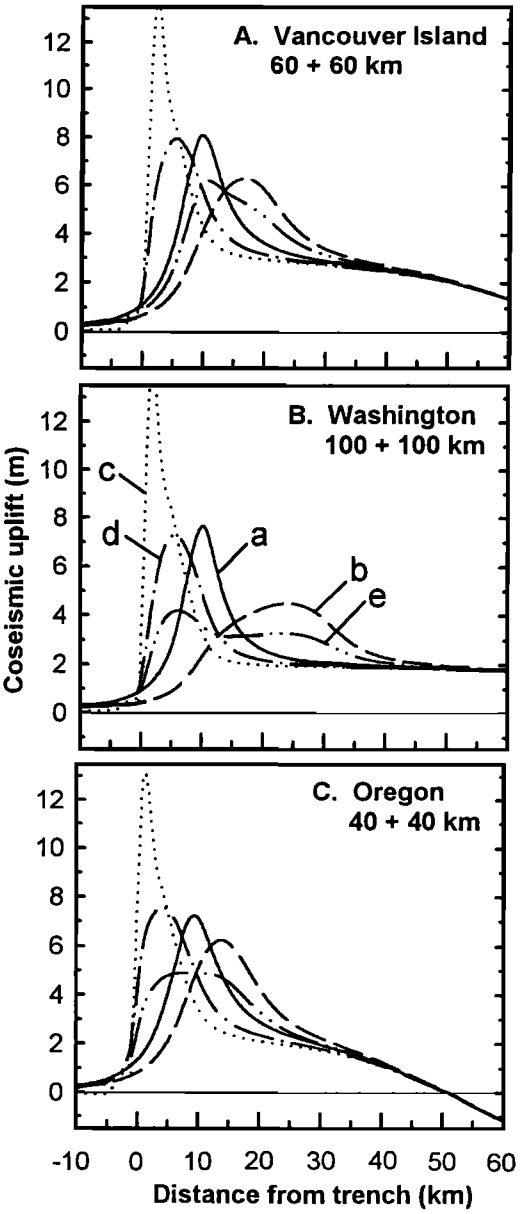

Figure 8. Predicted vertical coseismic deformation in the deformation front region for three profiles across the margin. The fault geometry is shown in Figure 7f and slip models are shown in Figures 7a-7e.

data uncertainties. A gap in the locked zone and thus a separation into a northern and southern part, a model examined by several authors [e.g., *Mitchell et al.*, 1994; *Verdonck*, 1995], is not needed to fit the available geodetic data. However, more complex locked and transition zones are not excluded.

There is a general correspondence between the pattern of coseismic subsidence along the coast and that estimated from coastal marsh paleoseismicity data. The dislocation model predicted subsidence for the most recent event (year 1700) ranges from about 0.5 m (central Oregon) to 2 m (Washington). These are similar to the subsidence inferred from coastal studies, i.e., least for central Oregon and most for northern Washington and southern Vancouver Island. However, the paleoseismicity data are not yet sufficiently quantitative to make an accurate comparison along the whole margin. This comparison is an important area for future work.

The poorly known slip geometry and coseismic slip distribution at the toe of the rupture zone reduce the precision of tsunami modeling. Sediment deformation may also be important near the toe of the deformation front.

With the new 3-D model routine the errors in modeled surface deformation due to inaccuracies in defining the fault dislocation are probably insignificant, and further efforts in elastic modeling will give small improvement. A significant improvement in modeling interseismic deformation requires a more realistic viscoelastic rheology. The variation in deformation rate through the interseismic period has yet to be monitored adequately, and the role of creep through the interseismic period is as yet unknown. The theoretical problems with our modeling of the coseismic deformation are less severe than for the interseismic period, but the "coseismic" deformation may result from slip at a range of timescales from rapid seismic rupture to slip over times of days to years. Our models provide no information on the dynamics of coseismic slip which are important to seismic wave and tsunami generation. Also, the degree to which the true rupture slip follows the simple theoretical coseismic slip distribution is unknown. Even if most of the fault zone ruptures in each great event, there may be more slip in one area for one earthquake, and more slip in a different area for a second event, such that the long-term multievent average is the same. There is evidence from southwest Japan that the coseismic rupture area in great events is reasonably approximated by the interseismic locked and transition zones from elastic dislocation modeling. However, the accuracy and consistency of this correlation among many great events need to be determined more accurately.

Based upon our model results, the moment magnitude for a great Cascadia earthquake is M_w=9.2 assuming there is complete rupture along the whole margin, as discussed by *Hyndman and Wang* [1995]. This result confirms that, like the Alaska and Chile plate margins, great subduction earthquakes will occur on the Cascadia margin.

Acknowledgments. We acknowledge very helpful discussions with R. McCaffrey, G. Priest, H. Dragert, and J. Henton. Y. Okada kindly provided the computer code for the point source and rectangular fault dislocation. A. Green arranged the Swiss Federal Institute of Technology thesis study for Paul Flück that resulted in this article. Geological Survey of Canada Publication Contribution #1996431.

References

Adams, J., Paleoseismicity of the Cascadia subduction zone: Evidence from turbidites off the Oregon-Washington margin, *Tectonics, 9*, 569-583, 1990.

Ando, M., and E.I. Balazs, Geodetic evidence for aseismic subduction of the Juan de Fuca plate, *J. Geophys. Res., 84*, 3023-3028, 1979.

Atwater, B.F., et al., Consensus about past great earthquakes at the Cascadia subduction zone, *Earthquake Spectra, 11*, 1-18, 1995.

Bostock, M.G., and J.C. VanDecar, Upper mantle structure of the northern Cascadia subduction zone, *Can. J. Earth Sci., 32*, 1-12, 1995.

Byrne, D.E., D.M. Davis, and L.R. Sykes, Loci and maximum size of thrust earthquakes and the mechanics of the shallow region of subduction zones, *Tectonics, 7*, 833-857, 1988.

Cassidy, J., A review of receiver function studies in the southern Canadian Cordillera, *Can. J. Earth. Sci., 32*, 938-951, 1995.

Cassidy, J., and R.M. Ellis, S-wave velocity structure of the northern Cascadia subduction zone, *J. Geophys. Res., 98*, 4407-4421, 1993.

Clague, J.J., and P.T. Bobrowsky, Evidence for a large earthquake and tsunami 100-400 years ago on western Vancouver Island, British Columbia, *Quat. Res., 41*, 176-184, 1994.

Clague, J.J., J.R. Harper, R.J. Hebda, and D.E. Howes, Late Quaternary sea levels and crustal movements, coastal British Columbia, Can. *J. Earth Sci., 19*, 597-618, 1982.

Crosson, R.S., and T.J. Owens, Slab geometry of the Cascadia subduction zone beneath Washington from earthquake hypocenters and teleseismic converted waves, *Geophys. Res. Lett., 14*, 824-827, 1987.

Davis, E.E., and R.D. Hyndman, Accretion and recent deformation of sediments along the northern Cascadia subduction zone, *Geol. Soc. Am. Bull., 101*, 1465-1480, 1989.

DeMets, C., R.G. Gordon, D.F. Argus, and S. Stein, Current plate motions, *Geophys. J. Int.*, 101, 425-478, 1990.

DeMets, C., R.G. Gordon, D.F. Argus, and S. Stein, Effect of recent revisions to the geomagnetic reversal time scale on estimates of current plate motions, *Geophys. Res. Lett., 21*, 2191-2194, 1994.

Douglass, J.J., and B.A. Buffett, The stress implied by dislocation models of subduction deformation, *Geophys. Res. Lett., 22*, 3115-3118, 1995.

Douglass, J.J., and B.A. Buffett, Reply to comment by J.C. Savage on "The stress implied by dislocation models of subduction deformation," *Geophys. Res. Lett., 23*, 2711-2712, 1996.

Dragert, H., and R.D. Hyndman, Continuous GPS monitoring of strain in the northern Cascadia subduction zone, *Geophys. Res. Lett., 22*, 755-758, 1995.

Dragert, H., and M. Lisowski, Crustal deformation measurements on Vancouver Island, British Columbia: 1976-1988, in *Global and Regional Geodynamics*, edited by P. Vyskocil, C. Reigber, and P.A. Cross, pp. 241-250, Springer-Verlag, New York, 1990.

Dragert, H., R.D. Hyndman, G.C. Rogers, and K. Wang, Current deformation and the width of the seismogenic zone of the northern Cascadia subduction thrust, *J. Geophys. Res., 99*, 654-668, 1994.

Flück, P., 3-D dislocation model for the great earthquakes of the Cascadia subduction zone, diploma thesis, 105 pp., Swiss Federal Inst. of Technol. (ETH), Zürich, Switzerland, 1996.

Geist, E., and S. Yoshioka, Source parameters controlling the generation and propagation of potential local tsunamis along the Cascadia margin, *Nat. Hazards, 13*, 151-177, 1996.

Green, A., R.M. Clowes, and R.M. Ellis, Crustal studies across Vancouver Island and adjacent margin, in *Studies of Laterally Heterogeneous Structures Using Seismic Refraction and Reflection Data*, edited by A.G. Green, *Geol. Surv. Can., Pap. 89-13*, 3-25, 1990.

Guibault, J-P., J.J. Clague, and M. Lapointe, Foraminiferal evidence for the amount of coseismic subsidence during a Late Holocene earthquake on Vancouver Island, west coast of Canada, *Quat. Sci., 15*, 913-937, 1996.

Henton, J. A., H. Dragert, and R.D. Hyndman, Continuous GPS monitoring of crustal deformation in the northern Cascadia subduction zone: An update, paper presented at meeting of Canadian Geophysical Union, Banff, Alberta, Canada, May 4-8, 1997.

Holdahl, S.R., R. Faucher, and H. Dragert, Contemporary vertical crustal motion in the Pacific Northwest, in *Slow Deformation and*

Transmission of Stress in the Earth, Geophys. Monogr. Ser., vol. 49, edited by S.C. Cohen and P. Vanicek, pp. 17-29, AGU, Washington, D.C., 1989.

Hyndman, R.D., The Lithoprobe corridor across the Vancouver Island continental margin: The structural and tectonic consequences of subduction, *Can. J. Earth Sci. 32*, 1777-1802, 1995.

Hyndman, R.D., and K. Wang, Thermal constraints on the zone of major thrust earthquake failure: The Cascadia subduction zone, *J. Geophys. Res., 98*, 2039-2060, 1993.

Hyndman, R.D. and K. Wang, The rupture zone of Cascadia great earthquakes from current deformation and the thermal regime, *J. Geophys. Res., 100*, 22,133-22,154, 1995.

Hyndman, R.D., C.J. Yorath, R.M. Clowes, and E.E. Davis, The northern Cascadia subduction zone at Vancouver Island: Seismic structure and tectonic history, *Can. J. Earth Sci. 27*, 313-329, 1990.

Hyndman, R.D., G. D. Spence, T. Yuan, and E.E. Davis, Regional geophysics and structural framework of the Vancouver Island margin accretionary prism, Proc. Ocean Drill. Program, Initial Rep., 146, 399-419, 1994.

Hyndman, R.D., K. Wang, and M. Yamano, Thermal constraints on the seismogenic portion of the southwestern Japan subduction thrust, *J. Geophys. Res., 100*, 15,373-15,392, 1995.

Hyndman, R.D., M. Yamano, and D.A. Oleskevich, The seismogenic zone of subduction thrust faults, *Island Arc*, in press, 1997.

Jachens, R.C., and A. Griscom, Three-dimensional geometry of the Gorda plate beneath northern California, *J. Geophys. Res, 88*, 9375-9392, 1983.

Kelsey, H.M., D.C. Engebretson, C.E. Mitchell, and R.L. Ticknor, Topographic form of the Coast Ranges of the Cascadia margin in relation to coastal uplift rates and plate subduction, *J. Geophys. Res., 99*, 12,245-12,255, 1994.

Lapp, D.B., R.S. Crosson, and T.J. Owens, P-waveform analysis for local subduction geometry beneath Puget Sound, Washington, *Pure Appl. Geophys., 133*, 349-365, 1990.

MacKay, M.E., G.F. Moore, G.R. Cochrane, J.C. Moore, and L.D. Kulm, Landward vergence and oblique structural trends in the Oregon margin accretionary prism: Implications and effect on fluid flow, *Earth Planet. Sci. Lett., 109*, 477-491, 1992.

Mitchell, C.E., P. Vincent, R.J. Weldon II, and M.A. Richards, Present-day vertical deformation of the Cascadia margin, Pacific Northwest, U.S.A., *J. Geophys. Res., 99*, 12,257-12,277, 1994.

Nabelek, J., X. Li, R. Fabritius, J. Braunmiller, B. Leitner, and A. Trehu, The structure of the Cascadia arc in central Oregon, Geol. *Soc. Am., Abstr. Programs, 28*, 95, 1996.

Okada, Y., Surface deformation due to shear and tensile faults in a half space, *Bull. Seismol. Soc. Am., 75*, 1135-1154, 1985.

Oleskevich, D., Constraints on the seismogenic zone in subduction thrust faults, M.Sc. thesis, 350 pp, Univ. of Victoria, Victoria, B.C., Canada, 1996.

Owens, T.J., R.S. Crosson, and M. A. Hendrickson, Constraints of the subduction geometry beneath western Washington from broadband teleseismic waveform modeling, *Bull. Seismol. Soc. Am., 78*, 1319-1334, 1988.

Priest, G.R., Explanation of mapping methods and the use of the tsunami hazard maps of the Oregon coast, *Oreg. Dep. Geol. Min. Ind. Open File Rep. O-95-67*, pp.1-95, 1995.

Rasmussen, J., and E. Humphreys, Tomographic image of the Juan de Fuca plate beneath Washington and western Oregon using teleseismic *P*-wave travel times, *Geophys. Res. Lett., 15*, 1417-1420, 1988.

Reilinger, R., and J. Adams, Geodetic evidence for active landward tilting of the Oregon and Washington coastal ranges, *Geophys. Res. Lett., 9*, 401-403, 1982.

Riddihough, R.P., Gorda plate motions from magnetic anomaly analysis, *Earth Planet. Sci. Lett., 51*, 163-170, 1980.

Riddihough, R.P., Contemporary movements and tectonics on Canada's west coast, *Tectonophysics, 86*, 319-341, 1982.

Riddihough, R.P., Recent movements of the Juan de Fuca plate system, *J. Geophys. Res., 89*, 6980-6994, 1984.

Rieken, E., and R.L. Thiessen, Three-dimensional model of the Cascadia subduction zone using earthquake hypocenters, western Washington, *Bull. Seismol. Soc. Am., 82*, 2533-2548, 1992.

Rogers, G.C., Earthquakes in the Vancouver area, in *Geology and Geological Hazards of the Vancouver Region, Southwestern British Columbia*, edited by J.W.H. Monger, *Geol. Surv. Can. Bull., 481*, 221-229, 1994.

Rohr, K.M.M., and K.P. Furlong, Ephemeral plate tectonics at the Queen Charlotte triple junction, *Geology, 23*, 1035-1038, 1995.

Satake, K., K. Shimazaki, T. Yoshinobu, and K. Ueda, Time and size of a giant earthquake in Cascadia inferred from Japanese tsunami records of January 1700, *Nature, 379*, 246-249, 1996.

Savage, J.C., A dislocation model of strain accumulation and release at a subduction zone, *J. Geophys. Res., 88*, 4984-4996, 1983.

Savage, J.C., Comment on "The stress state implied by dislocation models of subduction deformation" by J.J. Douglass and B.A. Buffett, *Geophys. Res. Lett., 23*, 2709-2710, 1996.

Savage, J.C., and G. Plafker, Tide gage measurements of uplift along the south coast of Alaska, *J. Geophys. Res., 96*, 4325-4335, 1991.

Savage, J.C., and W. Thatcher, Interseismic deformation at the Nankai Trough, Japan, subduction zone, *J. Geophys. Res., 97*, 11,117-11,135, 1992.

Savage, J.C., M. Lisowski, and W.H. Prescott, Geodetic strain measurements in Washington, *J. Geophys. Res., 86*, 4929-4940, 1981.

Savage, J.C., M. Lisowski, and W.H. Prescott, Strain accumulation in western Washington, *J. Geophys. Res., 96*, 14,493-14,507, 1991.

Smith, S.W., J.S. Knapp, and R.C. McPherson, Seismicity of the Gorda plate, structure of the continental margin, and an eastward jump of the Mendocino triple junction, *J. Geophys. Res., 98*, 8153-8171, 1993.

Snavely, P.D., Tertiary geologic framework, neotectonics, and petroleum potential of the Oregon-Washington continental margin, in *Geology and Resource Potential of the Continental Margins of western North America and Adjacent Basins -- Beaufort Sea to Baja California*, pp. 305-335, edited by D.W. Scholl, A. Grantz, and J. Vedder, Circum-Pac. Counc. for Energy and Min. Res., *Earth Sci. Ser.*, vol. 6, Houston, Tex., 1987.

Snay, R.A., and T. Matsikari, Horizontal deformation in the Cascadia subduction zone as derived from serendipitous geodetic data, *Tectonophysics, 194*, 59-67, 1991.

Spence, G.D., R.D. Hyndman, E.E. Davis, and C.J. Yorath, Seismic structure of the northern Cascadia accretionary prism: Evidence from new multichannel seismic reflection data, in *Continental Lithosphere: Deep Seismic Reflections, Geodyn. Ser.*, vol. 22, edited by R. Meissner et al., pp. 257-263, AGU, Washington, D.C., 1991.

Taber, J.J., and B.T.R. Lewis, Crustal structure of the Washington continental margin from refraction data, *Bull. Seismol. Soc. Am., 76*, 1011-1024, 1986.

Tanioka, Y., and K. Satake, Tsunami generation by horizontal displacement of the ocean bottom, *Geophys. Res. Lett., 23*, 861-864, 1996.

Thatcher, W., The earthquake deformation cycle at the Nankai Trough, southwest Japan, *J. Geophys. Res., 89*, 3087-3101, 1984.

Tichelaar, B.W., and L.J. Ruff, Depth of seismic coupling along subduction zones, *J. Geophys. Res., 98*, 2017-2037, 1993.

Trehu, A., I. Asudeh, T. Brocher, J. Luetgert, W. Mooney, J. Nabelek, and Y. Nakamura, Crustal architecture of the Cascadia forearc, *Science*, 266, 237-243, 1994.

Trehu, A., and the Mendocino Working Group, Pulling the rug out from under California: seismic images of the Mendocino triple junction region, *EOS Trans. AGU, 76*, 369, 384, 1995.

Verdonck, D., Three-dimensional model of vertical deformation at the southern Cascadia subduction zone, western United States, *Geology, 23*, 261-264, 1995.

Vrolijk, P., On the mechanical role of smectite in subduction zones, *Geology, 18*, 703-707, 1990.

Wang, K., Coupling of tectonic loading and earthquake fault slips at subduction zones, *Pure Appl. Geophys.*, 145, 537-559, 1995.

Wang, K., and G.C. Rogers, Double seismic layers in the subducted

Gorda plate and rheology of oceanic lithosphere, *Geophys. Res. Lett.*, *21*, 121-124, 1994.

Wang, K., H. Dragert, and H.J. Melosh, Finite element study of surface deformation in the northern Cascadia subduction zone, *Can. J. Earth Sci.*, 31, 1510-1522, 1994.

Wang, K., R.D. Hyndman, and M. Yamano, Thermal regime of the southwest Japan subduction zone: effects of age history of the subducting plate, *Tectonophysics, 248*, 53-69, 1995.

Weaver, C.S., and G.E. Baker, Geometry of the Juan de Fuca plate beneath Washington and Oregon from seismicity, *Bull. Seismol. Soc. Am., 78*, 264-275, 1988.

Westbrook, G.K., B. Carson, R.J. Musgrave, and Shipboard Scientists, *Proc. Ocean Drill. Program Initial Rep., 146*, 1994.

Wilson, D.S., Deformation of the so-called Gorda plate, *J. Geophys. Res., 94*, 3065-3075, 1989.

Wilson, D.S., Confidence intervals for motion and deformation of the Juan de Fuca plate, *J. Geophys. Res.*, 98, 16,053-16,071, 1993.

P. Flück, R. D. Hyndman, and K. Wang, Geological Survey of Canada, Pacific Geoscience Centre, P.O. Box 6000, Sidney, British Columbia V8L 4B2, Canada. (e-mail hyndman@pgc.emr.ca)

(Received January 10, 1997; revised May 26, 1997;
accepted June 4, 1997.)